AGU100 ADVANCING EARTH AND SPACE SCIENCE

Water Resources Research

RESEARCH ARTICLE
10.1029/2018WR022938

Key Points:
- We developed a method to estimate specific yield through a sequence of electrical resistivity tomography campaigns during a period of aquifer head drop
- Time-lapse electrical resistivity tomography was applied to map 2-D water content variations in the unsaturated zone
- We analyzed inversion artifacts and applied a constrained inversion to improve the results

Supporting Information:
- Supporting Information S1
- Data Set S1
- Data Set S2

Correspondence to:
S. Dietrich,
sebadietrich@ihlla.org.ar

Citation:
Dietrich, S., Carrera, J., Weinzettel, P., & Sierra, L. (2018). Estimation of specific yield and its variability by electrical resistivity tomography. *Water Resources Research*, *54*, 8653–8673. https://doi.org/10.1029/2018WR022938

Received 13 MAR 2018
Accepted 27 SEP 2018
Accepted article online 8 OCT 2018
Published online 5 NOV 2018

Estimation of Specific Yield and its Variability by Electrical Resistivity Tomography

Sebastian Dietrich[1,2], Jesús Carrera[3,4], Pablo Weinzettel[1,5], and Leonardo Sierra[1,2]

[1]Instituto de Hidrología de Llanuras "Dr. Eduardo J. Usunoff", Azul, Argentina, [2]Consejo Nacional de Investigaciones Científicas y Técnicas (CONICET), Buenos Aires, Argentina, [3]Hydrogeology Group (GHS UPC-CSIC), Instituto de Diagnóstico Ambiental y Estudios del Agua (IDAEA), Barcelona, Spain, [4]Consejo Superior de Investigaciones Científicas (CSIC), Madrid, Spain, [5]Comisión de Investigaciones Científicas de la Provincia de Buenos Aires (CIC), La Plata, Argentina

Abstract Specific yield (Sy) is defined as the average volume of water that can be drained, per unit surface of aquifer per unit drop of head. This parameter is of critical relevance for groundwater resources assessment, but its estimation suffers from numerous difficulties, including spatial variability, hysteresis, dependence on depth to water table, or delayed drainage. As a result, no widely accepted method is available for its estimation. Here we show that most of these difficulties can be overcome by using time-lapse electrical resistivity tomography (ERT) to map water content variations in response to phreatic level fluctuations. We applied the method to a synthetic example and to a real site in Argentina. Results demonstrate that the approach is robust and provides a picture of how, how much and where water is being released from the soil when aquifer heads drop, which is the ultimate goal of Sy concept. ERT produced some oscillations in estimated water contents, which we attribute to inversion artifacts. Still, the error analysis and the synthetic example suggest that the impact of spurious oscillations tends to cancel out during estimation of Sy, which supports the robustness of the method. Estimated Sy is sensitive to the petrophysical law. If the slope of this law is inadequate, calculated values of Sy may be biased, but their variability patterns are well captured by the method. What is clear is that Sy is a spatially and temporally variable parameter, whose estimation is difficult. ERT represents a possible avenue to evaluate Sy and its variability.

1. Introduction

Specific yield (Sy) is defined as the average volume of water that can be drained, per unit surface of aquifer per unit drop of head, from the column of soil or rock extending from the water table to the ground surface (Meinzer, 1923). Because of its relevance to estimate the available water resources of unconfined aquifers, Meinzer (1932) ranked it, together with permeability, as "the two hydrologic properties of greatest significance." But he qualified its estimation as a perplexing problem, which is best illustrated by the fact that he proposed seven methods to measure Sy. The concept is illustrated in Figure 1. Under equilibrium conditions, a soil moisture profile develops above a static water table, so that the capillary pressure head at a point is numerically equal to the elevation of that point above that water table. This soil water profile moves vertically as the water table displaces downwards or upwards. Sy is the volume of water, expressed per unit surface area and unit change in head, between the initial and final equilibrium profiles (dashed area in Figure 1a). Under these conditions, and assuming that the material is homogeneous, Sy simplifies to

$$Sy = \frac{1}{h_2 - h_1}\int_{h_1}^{ztop}(\theta(z|h_2) - \theta(z|h_1))dz = \theta_s - \theta_{re} \quad (1)$$

where $\theta(z|h_1)$ is the equilibrium water content when the water table elevation is h_1. The integral is ideally performed up to the surface, but in practice, it is restricted to the zero flux plane (ZFP; minimum water content elevation) to avoid the effect of near surface perturbations; θ_s is the saturated water content (porosity), and θ_{re} is the residual water content after drainage, often substituted in practice by field capacity. This is the drainable porosity, which is often used as synonymous of Sy, and represents a concept of practical value for many groundwater studies (Duke, 1972) because it allows treating Sy as a time-independent parameter that accounts for the instantaneous release of water from storage (Healy & Cook, 2002). This use implicitly assumes that drainage is complete and instantaneous at all points above the water table. However, this assumption is not valid in many practical situations.

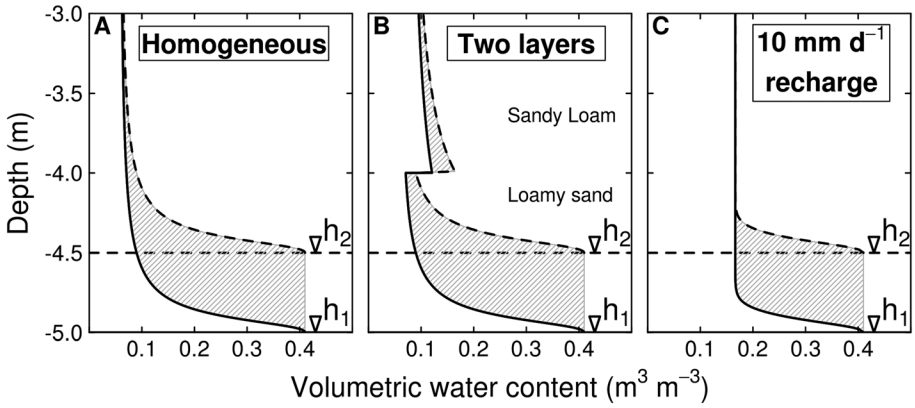

Figure 1. Equilibrium soil water content columns for (a) a homogeneous loamy sand, computed with van Genuchten (1980) parameters of Carsel and Parrish (1988) and water table at $h_1 = -5$ m (black line) and $h_2 = -4.5$ m (dashed line); (b) the same when the soil above $z = -4.0$ m is a sandy loam; (c) same as (a) but with a recharge of 10 mm/day. Specific yield (Sy) is ideally defined as the area (stripped) between the water contents for h_1 and h_2 divided by $(h_2 - h_1)$.

Equation (1) may not be valid when the water table is near the surface, so that the development of the static soil water profile may be restricted (Childs, 1960), which explains why Sy is often smaller in lowlands than in uplands (van Gaalen et al., 2013) and the rapid development of surface runoff after rainfall (Gillham, 1984). The hysteric behavior of the soil retention curve implies that the calculated Sy of a rising water table will not be the same as the calculated with a falling water table (dos Santos & Youngs, 1969; Duke, 1972), depending on the antecedent water content profile. These difficulties have prompted alternative definitions, such as the apparent Sy (Duke, 1972), the bulk Sy or virtual Sy (dos Santos & Youngs, 1969) in an attempt to express Sy as a function of field measurable quantities.

Equation (1) may also be inappropriate under recharge conditions when the water content profile is not hydrostatic (Figure 1c). Worse, when water table moves fast, the moisture distribution may lag behind, and reaching the new equilibrium conditions may take a certain time interval that depends on the soil type. Meinzer (1932) pointed out that it may take "several weeks." That is, complete drainage is never instantaneous, but delayed (dos Santos & Youngs, 1969; Healy & Cook, 2002).

Delayed yield complicates the interpretation of pumping tests, which would be the most natural field method to estimate Sy of unconfined aquifers over large areas. However, hydrologists soon noticed that Sy estimated from pumping tests are far smaller than implied by equation (1), which prompted the development of methods to account for delayed yield in the interpretation of pumping tests (Boulton, 1963; Neuman, 1975) or by calculating the ratio of cumulative volume of water pumped to the volume of the water table drawdown cone (Nwankwor et al., 1984; Remson & Lang, 1955). However, estimated values of Sy are highly sensitive to interpretation assumptions, such as whether the aquifer is anisotropic, or the pumping well fully penetrating (Neuman, 1975, 1979). Furthermore, Sy estimates often depend on the duration of the test, on distance to the observation point, or on characteristics of the soil and the observation well (Moench, 1994, 2008; Neuman, 1987). Models accounting for all these effects, including delayed drainage from the unsaturated zone have been developed (Mathias & Butler, 2006; Tartakovsky & Neuman, 2007), thus improving the estimation. However, to achieve significant drainage, pumping tests must be long which makes them costly. Worse, interpretation methods tend to neglect the heterogeneous nature of aquifers, which affect most notably the estimation of storage (Meier et al., 1998; Sanchez-Vila et al., 1999). In short, we fear that the conclusion of Neuman (1987) stating that pumping tests are not appropriate to estimate Sy remains valid.

Given the difficulties of traditional methods, more specific approaches have been developed to assess the variations of water content in the unsaturated zone. The most promising of these was the use of neutron probes, which are lowered in observation boreholes to determine vertical profiles of volumetric water content (Meyer, 1962) at several times during hydraulic tests or during the year (Silberstein et al., 2013). They worked well in producing profiles that look like those in Figure 1 (Loetz & Leake, 1983). The problem with neutron probes is that their use is heavily regulated, so that they cannot be used indiscriminately.

Changes in gravity over time can be used to estimate variations in groundwater storage in unconfined aquifers (El-Diasty, 2016; Gehman et al., 2009). This method allowed determining areal variations in hydraulic properties including Sy. However, a minimum of 0.3 m of water table variation is required to be reliably detected (Damiata & Lee, 2006). Moreover, an integration of Sy along vertical direction is obtained as a result, which prevents from discretization of vertical variation of Sy. In addition to this drawback, field procedures and data processing are laborious (Gehman et al., 2009).

Magnetic resonance sounding (MRS) is a promising method in hydrogeologic investigations because water molecules in aquifers generate a magnetic resonance signal that can be recorded (Legchenko & Valla, 2002). This interesting feature has motivated several studies intended to assess the links between the MRS parameters and the hydrogeological properties (e.g., Plata & Rubio, 2011; Vouillamoz et al., 2014; and many others). Today, although there is a strong theoretical basis for the relationship between MRS and aquifers parameters, no ready-to-use quantitative link has been proposed (Vouillamoz et al., 2007). On the other hand, MRS is a large-scale method that depends on the loop diameter and further research is required to improved noise reduction in data acquisition in 2-D and 3-D surveys (Legchenko & Valla, 2002).

Geoelectrical methods have been widely used to characterize flow dynamics in the unsaturated zone (Oberdörster et al., 2010; Rucker, 2009; Wehrer & Slater, 2015, and several more) and to assess hydraulic parameters such as permeability or transmissivity (Revil & Cathless, 1999; Niwas et al., 2011; among many others) as well as to monitor mass solute, mean solute advection and spreading (Singha & Gorelick, 2005). Despite the extensive literature on the relationship between resistivity and hydraulic properties, studies regarding Sy are less abundant. Frohlich and Kelly (1988) applied vertical electrical soundings (VES) to determine Sy by deriving a modification of Archie's law. They obtained good agreement with the Sy values obtained experimentally. Tizro et al. (2012) also employed VES surveys to evaluate Sy of the aquifer of Mahidashat plain, in Iran. The application of VES methodology implies that lateral variations in resistivity are disregarded.

The summary of this long discussion is that, while numerous methods have been tested, no one can be considered of universal use. In part, difficulties are associated to the basic difficulties of the Sy concept, using the words of Childs (1960): "The true solution of such problems will demand the study of the soil as a whole, both above and below the water table, as an essay in the field of water movement in a medium whose hydraulic conductivity is a function of moisture content." Geoelectrical methods, and specifically electrical resistivity tomography (ERT), appear promising in the sense that the unsaturated zone and aquifer are indeed considered as a whole. But they still require extensive testing and refinement. The objective of this work is to describe our efforts on the use of ERT to derive Sy.

2. Concepts

2.1. Hydraulics

The goal of this section is to revise quantitatively Sy and its conceptual difficulties, which motivate our work. The basic concepts behind Sy are derived from the flow equation which, assuming flow to be one-dimensional, reads

$$\frac{\partial \theta}{\partial t} = -\frac{\partial q}{\partial z} \tag{2}$$

where θ is volumetric water content and q is flux, which obeys the Darcy-Buckingham law

$$q = -K(\theta)\frac{\partial}{\partial z}(z - \psi) \tag{3}$$

where ψ is suction, usually taken to depend on θ through the retention curve (e.g., Hillel, 1998).

Properly accounting for transient effects (delayed yield) and hysteresis effects requires numerical solutions. But steady state solutions can be obtained easily for several simple cases. When the vertical flux can be neglected (e.g., after a long rainless period and static water table), then equation (3) implies that $z - \psi$ must be constant and equal to the elevation of the phreatic surface, h, where $\psi = 0$. Therefore, the water content profile, $\theta = \theta(\psi) = \theta(z - h)$, is identical to the retention curve, as shown in Figure 1a. The dashed area is the volume of water required to raise the water table from h_1 to h_2 (or drained when the water table drops from h_2

to h_1). The (static) water content profiles at $h_1$and h_2 are separated by $h_2 - h_1$. Therefore, assuming a sufficiently long soil column, the area equals $(h_2 - h_1)(\phi - \theta_f)$, where ϕ is porosity and θ_f is the field capacity, and $Sy = \phi - \theta_f$. This is the "drainable" porosity (also called "effective" porosity or "gravity" water porosity) and represents a frequent definition for Sy. It should be noticed that, close to the surface, the actual area may be a lot smaller (Childs, 1960).

Equation (3) can also be integrated easily for the case of constant recharge, r, in which case the water content profile (Figure 1b) can be obtained as

$$\psi(z) = \int_h^z \frac{K(\theta) - r}{K(\theta)} dz \tag{4}$$

Integration of the area between the water content profiles at $h_1$and h_2 can also take advantage of the fact that they are separated by $h_2 - h_1$, and Sy becomes $Sy = \phi - \theta_r$, where θ_r is the water content for a gravity flux equal to recharge (i.e., $K(\theta_r) = r$), which is apparent in Figure 1c. In reality, recharge may take place through preferential flow paths or through fingers, but the fact remains that the profile will be significantly wetter than under no-flow conditions, so that Sy will be much smaller than drainable porosity.

In summary, the actual value of Sy depends on antecedent conditions prior to head fluctuations, on the rate of head change, on the rate of recharge, etc. These difficulties are increased by heterogeneity and the fact that flow will rarely be strictly vertical. One might be tempted to conclude that the concept is hopeless, but the truth is that it is too useful and needed to ignore. Therefore, we must seek ways to estimate it.

2.2. Soil Resistivity and Petrophysical Laws

Electrical resistivity tomographty yields the spatial distribution of resistivities. For the estimation of Sy (equation (1)) we need the spatial distribution of water contents. These are related to resistivities by means of petrophysical laws, which we describe below. Resistivity, ρ, is an intrinsic property of materials which expresses their ability to oppose a flow of electrical charge. For an isotropic material, ρ is defined simply as the reciprocal of conductivity, σ, which in turn is the constant of proportionality between current density and the applied electric field intensity. Resistivity of water bearing sediments depends on water content and its salinity, temperature, and composition and arrangement of soil particles (Friedman, 2005). Many empirical models have been proposed to relate all these variables to bulk resistivity (Archie, 1942; Linde et al., 2006; Winsauer et al., 1952; and many others, see review by Friedman, 2005). Among these models, Archie's law has been extensively used:

$$\rho_b = a\phi^{-m}S^{-n}\rho_w \tag{5}$$

where ρ_b is bulk resistivity, ρ_w is water resistivity, S, is saturation, and a, m and n are empirical parameters. Parameters m and n are usually termed cementation factor and saturation exponent, respectively. It should be noted that Archie's law, in its original form, did not include the empirical factor a (see discussion by Glover, 2015).

The term formation factor, F, is usually employed to denote the ratio of ρ_b to ρ_w. Shah and Singh (2005) rearranged equation (5) to write it in terms of water content $\theta = S\phi$. Assuming that $m = n$, which reflects that these parameters often take similar values (Rinaldi & Cuestas, 2002), leads to

$$\frac{\rho_w}{\rho_b} = c\theta^n \tag{6}$$

This model, which is identical to Winsauer's model for the particular case of $m = n$, is especially attractive due to the reduced number of parameters. Parameter c, which replaced $1/a$ in equation (5), is related to the surface conductivity of solids and therefore should increase with clay proportion. Parameter n is related to the tortuosity of pore space. A problem with this model is that it does not work for pure water (i.e., when $\theta = 1$, ρ_b only equals ρ_w when $c = 1$). This and other limitations point out that Winsauer's law must be taken as an empirical law, valid only within the range of calibration.

To account for surface conduction, another petrophysical model was developed by Frohlich and Parke (1989) that, in the form proposed for fitting, reads

$$\frac{C_b}{C_{sat}} = \frac{\rho_w}{\rho_b} = S^n + \frac{1}{M} \tag{7}$$

where $M = C_s/C_{sat}$ and C_s is the conductivity of the solid medium (surface conduction), C_b is the bulk conductivity and C_{sat} is the conductivity at saturation. Note that both equations (6) and (7) highlight that, for uniform soils where variability of porosity and water resistivity can be neglected, bulk resistivity is basically a function of water content. The water content profile at several times can be obtained from resistivity profiles, which can be computed through ERT surveys, as explained below.

2.3. ERT

The aim of electrical surveys is to determine the subsurface resistivity distribution by performing measurements from the surface or from a borehole. Electrical current is injected into the ground by means of two electrodes and the resulting voltage is measured with another pair of electrodes (the set of four electrodes is called quadrupole). Electrodes may be arranged in different manners, termed electrode arrays, each one with different resolution abilities. In traditional 1-D VES, distances between electrodes are increased sequentially to increase the depth of investigation at each step, but neglecting horizontal variation (Samouëlian et al., 2005). Accounting for lateral variations in resistivity requires ERT surveys, which are performed by simultaneously installing a large number of electrodes connected to a control center by means of a multicore cable. At each step, the control center automatically selects a quadrupole for measurement. Spatial variability of resistivity can be estimated through inversion (i.e., the process of finding the resistivity model that best fits the whole sequence of quadrupole measurements). Inversion is a nonlinear problem that has to be solved numerically using iterative procedures (Tripp et al., 1984). To avoid ambiguity, in this paper we talk about "real resistivities", when referring to the unknown reality, "computed resistivities" when referring to those resulting from inversion and "apparent resistivities" (both "real" and "computed") when describing the ones resulting from direct voltage measurements interpreted assuming a homogeneous medium (i.e., voltage divided by current intensity times a geometric factor).

The ERT inverse problem is "ill-posed" (sometimes referred to as ill-constrained or underdetermined) in that the solution may be non-unique or unstable. Therefore, regularization is needed to remove or, at least, to reduce the ambiguity of the solution (Günther, 2004), which leads to an objective function, **S**, to be minimized, of the form:

$$S(\mathbf{m}) = F_d(\boldsymbol{\varepsilon}) + \lambda F_m(\mathbf{m}) \tag{8}$$

where $F_d(\boldsymbol{\varepsilon})$ measures model fit and $F_m(\mathbf{m})$ measures the plausibility (regularization) of estimated model parameters, $\mathbf{m}$; $\boldsymbol{\varepsilon} = \mathbf{W_d}(\mathbf{d}_{obs} - \mathbf{g}(\mathbf{m}))$ is the vector of weighted model errors; $\mathbf{d}_{obs}$ is the vector of observed data and $\mathbf{g}(\mathbf{m})$ is the vector of corresponding model computations (model response), which depends on model parameters; $\mathbf{W_d}$ is the matrix used to weight data, and λ is the Lagrange multiplier or regularization parameter that determines the importance given to the plausibility of the estimation. The model fit function, $F_d(\boldsymbol{\varepsilon})$, is often written as a sum of squared errors (i.e., $F_d(\boldsymbol{\varepsilon}) = \boldsymbol{\varepsilon}^T\boldsymbol{\varepsilon}$, L_2 norm). This type of function is known to be sensitive to outliers, which penalize heavily the objective function and may degrade the estimation by striving to reduce the contribution of outliers. To overcome this problem, robust methods use the absolute value of models errors (i.e., $F_d(\boldsymbol{\varepsilon}) = \sum_i|\epsilon_i|$, L_1 norm) (Claerbout & Muir, 1973; Loke et al., 2003). On the other hand, a number of possibilities are available for F_m. A frequent choice is the "smooth inversion", where $F_m(\mathbf{m}) = \mathbf{m}^T\mathbf{Rm}$, with **R** a roughness matrix. Effectively, this type of F_m penalizes the contrast in resistivity among adjacent blocks and tends to yield smooth electrical resistivity fields (deGroot-Hedlin & Constable, 1990). Farquharson and Oldenburg (1998) discuss alternatives to produce more "blocky" appearances (structured models with regions of almost constant resistivities separated by sharp boundaries). These functions rely heavily on the use of available prior information to improve the identifiability of resistivities and will generally improve results if such prior information is correct, but may worsen it if not (Carrera & Neuman, 1986; Ellis & Oldenburg, 1994). Therefore, parsimony (select the simplest model that explains the data) favors smooth inversion, unless strong arguments exist for another choice.

When studying dynamic changes in some particular subsurface property, a time-lapse survey (i.e., repeat ERT surveys at a sequence of times) is frequently adopted. Time-lapse inversion is appropriate when the modeler is more interested in resistivity changes than in the overall resistivity itself, because changes are less sensitive to systematic errors (i.e., in the measurement equipment, the location of electrodes, or the like) than the overall resistivity field. A number of methods have been developed to handle time-lapse data (Ellis & Oldenburg, 1994; Hayley et al., 2011; Loke et al., 2014; Miller et al., 2008; Oldenborger et al., 2007).

3. Proposed Method for Estimation of Sy and Error Analysis

3.1. Methodology

The approach consists of three steps:

Step 1: **Time-lapse ERT.** Surveys should be carried out during periods when significant head drop and/or head rise is expected, so as to maximize soil water differences while allowing for planning the ERT campaigns. In places where recharge is maximum during winter, ERT surveys should be performed during summer and fall, while head drop is monitored. Alternatively (or complementarily), head rise monitoring and ERT surveys can be performed during winter and spring. Furthermore, if ERT surveys are performed immediately after a rain event, soil water content may be affected by recharge fluxes (leading to a low Sy, recall Figure 1c) or by preferential recharge paths. These effects may be of interest for studying the nature of recharge, but they will hinder the estimation of long term Sy, which is the one needed for water management. Therefore, ERT surveys should be performed after a few rainless days.

Step 2: **Derivation of volumetric water contents from resistivity** using petrophysical laws, such as equations (6) and (7), or any other one that the modeler considers appropriate.

Step 3: **Evaluation of Sy from changes in water content and head.** This is performed by integrating water content profiles along the ERT transect using equation (1), as outlined in Figure 1, which yields Sy as a function of distance along the transect. This can be achieved, for each column of cells, by adding up the water content change multiplied by the cell height for all cells between the water table and the ZFP (i.e., the elevation, z, where $\partial\theta/\partial z = 0$). The water table does not need to coincide with a cell edge. This, together with the expected overall monotonicity and relatively smooth dependence of water content with z, suggests that integration be performed by interpolating water contents.

3.2. A First-Order Error Analysis on the Estimation of Sy

The estimation of Sy in Step 3 above can contain errors because of either inversion errors in bulk resistivity, ε_ρ, or errors in the petrophysical function ($\theta = \varphi(\rho_b)$). The latter can be caused by conceptual errors (e.g., unduly neglecting variability of ρ_w due to salinity or temperature variations), by a poor choice of the functional dependence (e.g., choice of equations (6) or (7)), or by errors in the parameters of the chosen petrophysical law. As we shall see below, the functional form is not critical for Sy (although it may for other purposes involving θ). Therefore, we concentrate on parametric uncertainty and choose equation (6) to illustrate the nature of errors. Solving equation (6) for θ, differentiating and using again equation (6) to eliminate ρ_b, allows us to write the error in θ as

$$\varepsilon_\theta = \frac{\partial\theta}{\partial\rho}\varepsilon_\rho + \frac{\delta\theta}{\delta\varphi}\varepsilon_\varphi = -\frac{c\theta^{n+1}}{n\rho_w}\varepsilon_\rho - \frac{\theta \ln\theta}{n}\varepsilon_n - \frac{\theta}{nc}\varepsilon_c \tag{9}$$

where ε_n, and ε_c are the errors in parameters n and c, respectively. To illustrate this equation, let us assess the impact of neglecting temperature or salinity variations, which affect ρ_w. Errors in ρ_w translate linearly into errors in ρ_b (equation (6)), so that $\varepsilon_{\rho w}/\rho_w = \varepsilon_\rho/\rho_b$. Using this and substituting equation (6) into equation (9), $\varepsilon_\theta/\theta = -(1/n)\varepsilon_{\rho w}/\rho_w$. Adopting the standard sensitivity of 2% reduction in water resistivity per °C, a value of $n = 2$ would imply a 1% error in water content per °C error in temperature. A similar analysis could be made for salinity.

Substituting equation (9) in equation (1) leads to the error in Sy, ε_{Sy}. To obtain workable approximations, we work under ideal static conditions and approximate the integrand of the resulting expression as $\varepsilon_\theta(z|h_2) - \varepsilon_\theta(z|h_1) = (\partial\varepsilon_\theta/\partial z)(h_2 - h_1)$, which leads to an immediate integral and

$$\varepsilon_{Sy} = \varepsilon_{\phi} - \varepsilon_{\theta f} \tag{10}$$

where ε_{ϕ} is the error in θ at the water table (saturated water content, which we take as porosity, ϕ) and $\varepsilon_{\theta f}$ is the error corresponding to elevations far above the water table (field capacity). Note that (1) equation (10) is quite trivial (under the assumed conditions, $Sy = \phi - \theta_f$), (2) under more general conditions, $\varepsilon_{\theta f}$ needs to be substituted by the error at the upper integration limit (normally, the ZFP), and (3) the error is independent of the form of the adopted petrophysical law. It also points out that, as long as resistivity is a monotonic function of θ, errors in the petrophysical relationship will tend to cancel because errors in porosity (ε_{ϕ}) will be of the same sign as those in field capacity ($\varepsilon_{\theta f}$). Substituting equation (9) in equation (10) allows us to isolate the errors on Sy caused by resistivity inversion errors ($\varepsilon_{Sy/\rho}$) and by those in the petrophysical law ($\varepsilon_{Sy/n}$ and $\varepsilon_{Sy/c}$), which become, respectively:

$$\varepsilon_{Sy/\rho} = -\frac{c}{\rho_w}\left(\phi^{n+1}\varepsilon_{\rho s} - \theta_f^{n+1}\varepsilon_{\rho f}\right) \tag{11}$$

$$\varepsilon_{Sy/n} = \frac{\theta_f \ln\theta_f - \phi \ln \phi}{n}\varepsilon_n = -\frac{Sy \ln(\phi - Sy) + \phi \ln[\phi/(\phi - Sy)]}{n}\varepsilon_n \tag{12}$$

$$\varepsilon_{Sy/c} = -\frac{Sy}{nc}\varepsilon_c \tag{13}$$

where $\varepsilon_{\rho s}$ is the resistivity error at the water table, and $\varepsilon_{\rho f}$ is the resistivity error at the upper integration limit (assumed to reach field capacity conditions). These equations point out that errors in Sy should be a relatively smooth function of errors in coefficient c, exponent n, or resistivity. In fact, if resistivity errors are correlated, so that $\varepsilon_{\rho s} \approx \varepsilon_{\rho f}$, equation (11) implies that the impact of inversion errors should be small. Trying different values of Sy and ϕ in equation (12) shows that the coefficient of ε_n in equation (12) is positive, whereas that of ε_c in equation (13) is negative. If the parameters have been calibrated, ε_n and ε_c should be positively correlated and thus display the same sign. Therefore, errors in Sy caused by errors in the petrophysical parameters will also tend to cancel. In summary, the error analysis suggests that the proposed method is robust in that estimated Sy should not be very sensitive to inversion errors (assuming that they are positively correlated from one survey to another) or petrophysical law errors (assuming that the petrophysical law has been calibrated).

Equations (11)–(13) represent an idealization because they are only a first-order approximation and because they assume static conditions. Full errors under conditions similar to those expected in reality are analyzed on a synthetic example below.

3.3. A Synthetic Example to Explore the Impact of Inversion and Petrophysical Parameters Errors on Sy Estimation

We did a synthetic example to assess the impact of inversion errors on the estimation of Sy. The procedure consisted of the following steps.

1. Generation of synthetic soil water content fields. We generated a spatially varying field of water content, assuming static conditions and spatially variable van Genuchten (1980) parameters. Spatial variability patterns are those of Figure 3 of Willmann et al. (2008), which had been generated using a power law variogram. This field was linearly scaled to represent spatially varying fields of van Genuchten (1980) parameters α (between 0.005 and 0.02 cm^{-1}) and n' (between 1 and 2) over a 55-m-long and 4-m-in depth grid, with 0.2×0.2 m^2 grid cells size. These parameters and synthetic survey size are comparable to those of our site (Dietrich et al., 2014). Using these parameters we computed soil water contents for two water table positions, 1.5 and 2.6 m below surface assuming a residual saturation of 0.15 and a porosity of 0.45 (Figures 2a and 2b, the actual water content values are available in the supporting information).
2. "Real" resistivities were computed from water contents using Shah and Singh's law (equation (6)) with $\rho_w = 6.06$ ohm·m, $c = 2.45$, and $n = 2.14$, which are the ones at the site we will describe in section 4.
3. ERT data acquisition was simulated by forward modeling of a 56-electrode Schlumberger array, with an offset of 1 m between electrodes, using a solution grid with the same size as the synthetic water content and resistivity fields. The computed values of V/I (voltage over current) were contaminated with a normalized random noise sequence to represent measurement errors. We used the same noise sequence for the high and low water table surveys to acknowledge that the main sources of errors are systematic

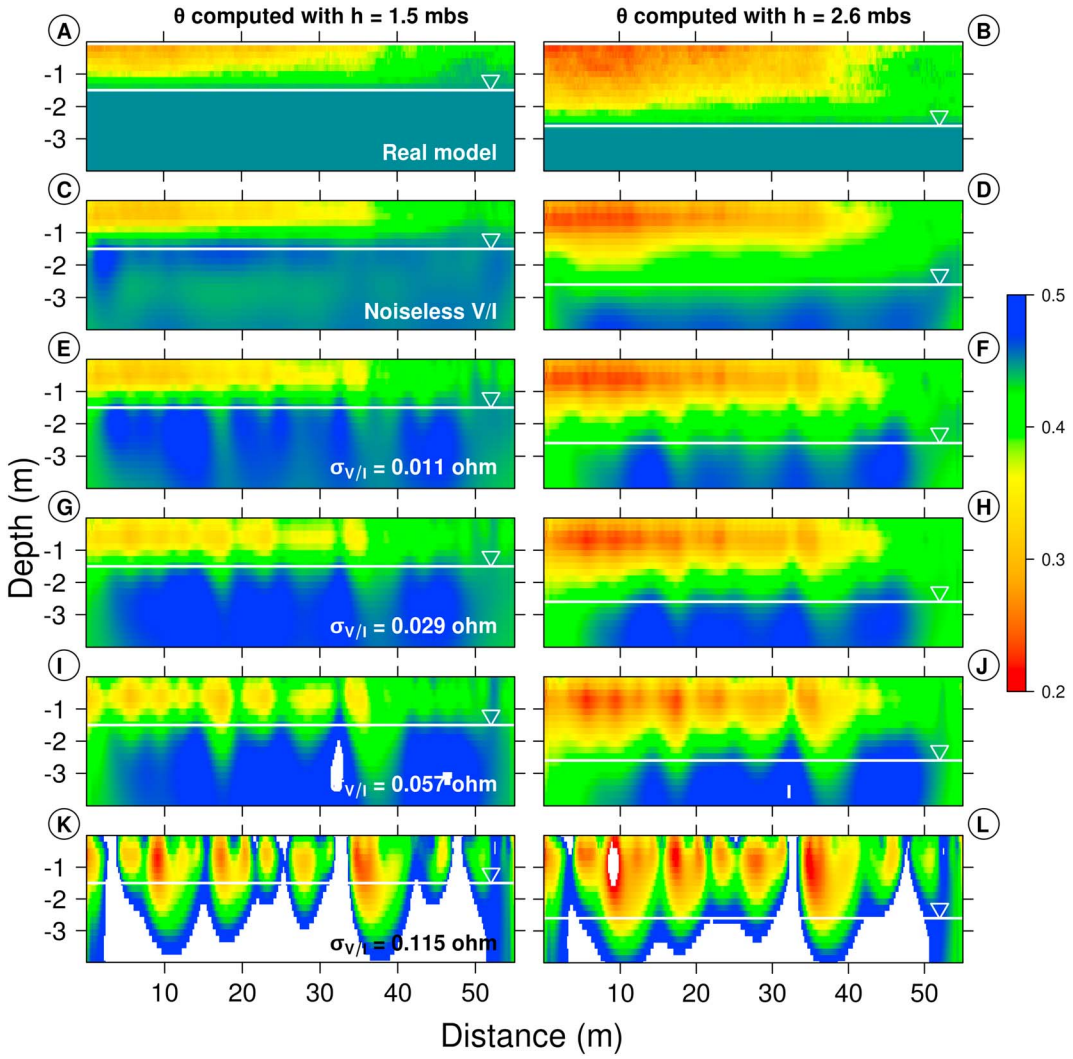

Figure 2. Real synthetic water contents (top row) and those resulting from electrical resistivity tomography with increasing levels of noise (descending rows). Results are displayed for the water table at 1.5 mbs (meters below surface, left column) and 2.6 mbs (right column). White zones indicate water contents beyond the scale limits.

(Oldenborger et al., 2005; Slater et al., 2000; Wilkinson et al., 2008; Zhou & Dahlin, 2003). We linearly transformed the noise sequence to generate five noisy data sets of V/I for high and low water tables, with standard deviations equal to 0, 0.011, 0.029, 0.057, and 0.115 ohm. For comparison, standard deviations of measured resistances typically are around 1 ohm, whereas the mean field reciprocal error ranged about 0.001 ohm (see below in section 4.2). While even the lowest noise is far greater than the actual error measured during field operations, we must point that the reciprocal error only quantifies errors during intensity and voltage measurements, which should be uncorrelated and small, whereas our noise is meant to represent random but systematic (that is, the same error across sequential surveys) errors, whose magnitude is hard to assess. Still, we also analyzed the effect of uncorrelated measurements errors by contaminating them with a random noise in a 80/20 ratio (systematic to uncorrelated ratio). This was accomplished by adding the above systematic errors, multiplied by 0.8, to a different noise for the two heads multiplied by 0.2.

4. We inverted synthetic apparent resistivities (noiseless and noisy) using smooth inversion with L_1-norm as the model fit criterion. We carried out one inversion per noise level. Resistivity inversions (not shown) reproduced the overall resistivity patterns of Figure 7 (larger resistivity above than below and larger resistivities for low than for high water level) and the lateral variability of the real resistivity maps, but instability lobes became apparent for inversion of data with standard deviations above 0.029 ohm.

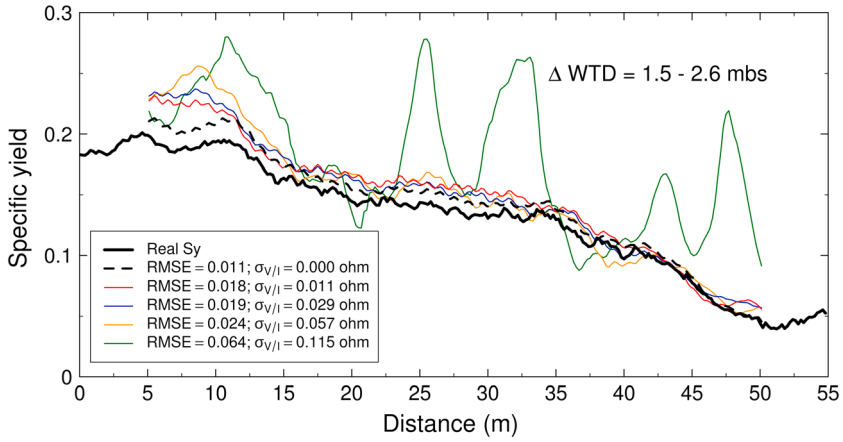

Figure 3. Estimation of Specific yield for the "real" and "computed" soil water content sections derived from electrical resistivity tomography surveys. RMSE = root-mean-square error; WTD = water table depth.

5. We converted resistivities to soil water contents using Shah and Singh's law (equation (6)) with the parameters of step 2 (the impact of uncertainty in these parameters is analyzed below), which yielded the water content images shown in Figure 2. Again, results generally reproduce the variability patterns of the true water contents (top row in Figure 2), but instability lobes (visually less marked than in resistivity images) become apparent for noises of 0.057 and 0.115 ohm standard deviation. As discussed in section 3.1, it is important for the calculation of Sy to note that estimation errors (discrepancies between computed and real water content maps) display similar trends (the lobes are located in similar positions) for the high and low water tables. Note that estimated water contents are too low at x = 0, 12, 18, 28, 37, and 55 m and too high at x = 6, 15, 25, 32, 42, and 48 m for both high and low water levels. This is true for all noise levels, including the noiseless inversion (!), which suggests that inversion results are affected not only by the noise but also the location of electrodes and the nature of resistivity inversion (simulated resistance being more sensitive to some spatial averaging of resistivity than to its point values).
6. Sy was computed for every x value using equation (1). The resulting Sy(x) curves are shown in Figure 3. All calculations reproduce the spatial variability of the true Sy and are qualitatively good, much better than the computed water contents of Figure 2, which reflects that errors in water contents are highly correlated, so that errors in Sy are modest. This is further supported by the paradoxical observation that the estimations of Sy with the various levels of noise are only slighty worse than those obtained with noiseless data (affected by round-off errors), even though the estimation of water contents degraded with increasing noise (Figure 2). High correlation of inversion errors between sequential surveys can be attributed to the systematic nature of measurement errors. In fact, when a different random component of noise (20% of the total error) was added to V/I measurements of each campaign, Sy estimates degraded a bit (see the supporting information). In essence, the point is that Sy estimation integrates the inversion and subtracts inversions from sequential surveys. Integration causes high-frequency inversion errors to cancel. Subtraction causes systematic errors to cancel as well, as implied by equation (11). As a result, Sy estimates turn out to be quite robust with respect to inversion errors.

We followed a similar approach to analyze the impact of errors in the petrophysical law. Thus, we started with the resistivities obtained after inversion of the noiseless V/I (with the "correct" Shah and Singh's parameters, these resistivities lead to the water contents shown in the second row of Figure 2). These resistivities still had some errors due to round-off errors in the resistances (their impact on water contents computed with correct Shah and Singh's parameters can be assessed by comparing the two top rows in Figure 2). In order to evaluate the impact of uncertainties of Archie's parameters on computed Sy, we sampled randomly different sets of c and n parameters from the expected interval of variation, that is, 1 to 3 (Rinaldi & Cuestas, 2002; Shah & Singh, 2005), whereas ρ_w remained constant at the same value as before, that is, 6.06 ohm·m. We used these parameters in equation (6) to obtain water contents, which we integrated as before for every x (equation (1)) to obtain Sy(x). The results are shown in Figure 4, which also displays the root-mean-square error with respect to the real Sy.

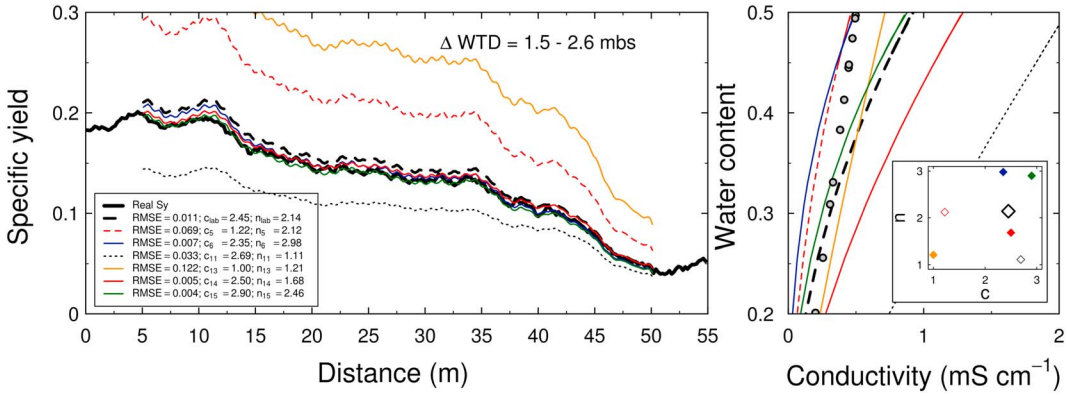

Figure 4. (left) Specific yield computed from the synthetic resistivity survey using several sets of modified Archie's law parameters. (right) Dependence of water content on bulk conductivity for the same sets (dots are the experimentally measured values), which are plotted (*c* vs. *n*) in the inset. RMSE = root-mean-square error.

Figure 4 illustrates equations (12) and (13) in that (1) errors in Sy are moderate when errors in the parameters are small, (2) errors are proportional to Sy, and (3) the spatial variability of Sy is well captured by all models. Still, the errors in the estimation of mean Sy are somewhat puzzling. On the one hand, a petrophysical law (e.g., the yellow one with $c = 1$ and $n = 1.21$), which is quite close to the true one (dashed black line), yields far too high Sy values. On the other hand, the red (2.50, 1.68) or blue (2.35, 2.98) petrophysical laws, which are far from the true one, lead to almost perfect Sy values. These results imply that (1) attention must be paid to the calibration of the petrophysical law and (2) what controls Sy is the difference between the water contents near saturation and near field capacity. The corresponding bulk conductivities in this case are 0.92 and 0.12 mS/cm, respectively. With those conductivities, the red law would have yielded too low water contents, which would have been too high for the blue one (but their difference along each vertical would have been correct!). Similarly, the yellow law would have led to too low water content near field capacity and too high near saturation. An alert soil scientist should have identified the problem and correct the law. But this observation also suggests that the joint use of other types of data, or a joint inversion allowing us to estimate the parameters of the petrophysical law, may improve the approach.

The results displayed in Figures 3 and 4 confirm the findings of section 3.2 in that the estimation of Sy is quite robust. While the mean value of Sy can be affected by a poor choice of petrophysical parameters, the patterns of spatial variability are well resolved in all cases. These findings are in contrast to those of Singha and Gorelick (2005) for the estimation of point values of concentration, which reflects the integral nature of Sy.

4. Application to a Real Site

4.1. Study Site

The study was carried out next to an experimental plot located in a rural area near Azul city (36°46′S, 59°53′W), Buenos Aires, Argentina (Figure 5a). The site is located within the Azul Creek basin, in the Pampean plain region. The region consists of a thick cover of loess deposits, parent material of the modern cultivated soils (Zárate, 2003). The level ground of this region leads to a flat land hydrological system (Usunoff et al., 1999).

The soil has been classified as a petrocalcic Paleudol (Soil Survey Staff, 1999). At the top of the soil profile, there is a clayey loam A horizon with moderate to strong granular structure up to 18-cm depth. From 18- to 43-cm depth, there is a Bt horizon that is clay textured with strong and firm coarse columns and abundant clay films. The BCk horizon below extends up to 66-cm depth, with a silty clay texture, moderate medium to fine subangular blocks with $CaCO_3$ concretions. Finally, from 66- to 140-cm depth there is a Ck horizon, silty loam, very firm and massive, with variable CaCO3. Between 90 and 120 cm, there is a Ckm horizon (locally known as "tosca"), which is more enriched in $CaCO_3$ than the Ck horizon. It is common that Ckm occurs as massive, layered, or laminar bodies embedded in a more friable matrix, which resembles Ck material. Together, Ckm and the matrix (Ck) can be treated as the petrocalcic horizon as a whole with variations in CaCO3 proportions, degree of induration, and structure. From 140 cm up to 10 m depth (core sampling is available but not shown here), the subsurface consists of silty loessic sediments, also with an important

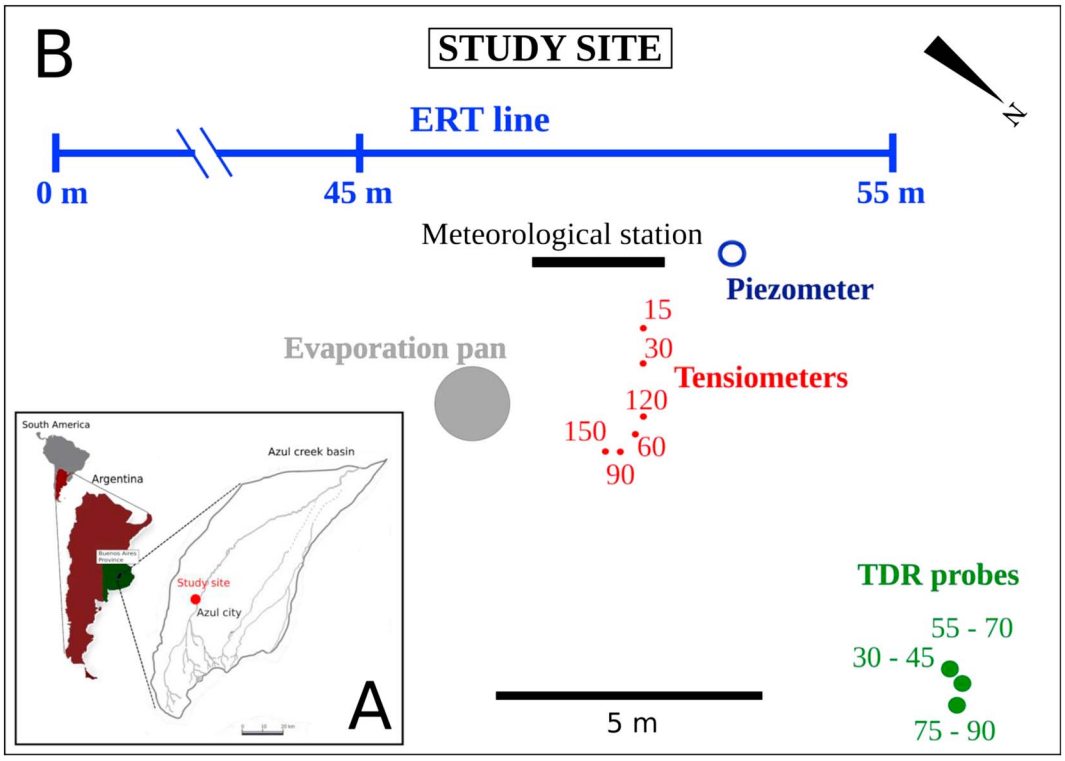

Figure 5. (a) Location of study site. (b) ERT line in relation to the location of measurement devices. Note that only ERT line length is out of scale (truncated). Besides that, distances of measurement devices to ERT line are at scale. ERT = electrical resistivity tomography; TDR = time domain reflectometry.

proportion of $CaCO_3$. These sediments compose the Pampeano aquifer unit that behaves as an unconfined aquifer. It is a common situation that thin clay layers are intermixed within loessic sediments, which results in a strong vertical anisotropy (Varni & Usunoff, 1999). Although lateral variability within each soil horizon is expected, horizons keep their identity laterally, as confirmed by the experience gained during site instrumentation. In addition, auger holes were drilled to test petrocalcic horizon continuity and hardness (Weinzettel et al., 2009).

The experimental plot is equipped with tensiometers, time domain reflectometry (TDR) probes, a piezometer, and an automatic meteorological station (Figure 5b). Tensiometers are located at 15, 30, 60, 90, and 150 cm in depth and enable flow direction and zero flow plane to be estimated. TDR probes are 15 cm in length and cover the following depth ranges: 30–45, 55–70, and 75–90 cm. Such probes allow estimation of volumetric water content. On the other hand, suction cups, located at the same depth as tensiometers, allow pore water extraction and electrical conductivity measurements. A 10-m deep piezometer with a screen at its bottom monitors water table depth. This piezometer is sampled every 6 months since 10 years ago.

4.2. Methodology

Step 1: Time-lapse ERT measurements were conducted beside the experimental plot (Figure 5b) between 17 September 2014 and 27 April 2015, when the water table fell almost monotonically from 0.71 to 3.21 m below surface (mbs) (Figure 6). This large head drop is due to natural seasonal fluctuation. The previous (austral) winter had been anomalously wet and there is no water exploitation affecting this part of the aquifer.

In total, nine tomography surveys (black triangles in Figure 6) were carried out, but only four (T1 to T4 in Figure 6) are used here to ensure a large water level change between sequential surveys for the estimation of Sy. Surveys were carried out with an AGI SuperSting R1/IP equipped with 56 electrodes. The Schlumberger setup was adopted to monitor resistivity changes along a 55-m-long transect (Figure 5b) and 488 data, distributed in 10 pseudosection levels, were collected in each survey. Electrodes were separated 5 m in the first survey (T1) and 1 m in the remaining. We had to reduce the electrode spacing after the first survey to gain

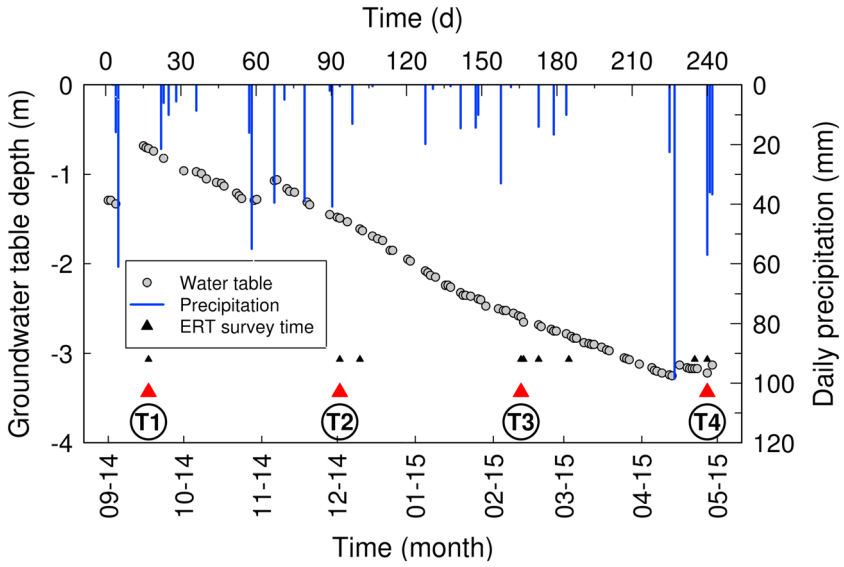

Figure 6. Water table drop and daily precipitation during study period. Times of ERT surveys are identified by black triangles. Only those labeled (red triangles) are used in this work. ERT = electrical resistivity tomography.

resolution at depth. In hindsight, it is clear that the same spacing (in fact, the same electrodes) with small spacing should be used from the beginning because inversion artifacts that result from resolution differences are going to be projected into the following inversions. As it was, we brought the first data set into the same scale as the later on by interpolation of the inverted results (see below to inversion details), that is, we reduced the original grid cells to match that ones of the following surveys.

In order to guarantee the quality of acquired data, measurements with misfit larger than 2% between normal and reversed polarity readings were repeated. A second evaluation of data quality was performed by means of the following criteria: minimum voltage (0.2 mV), minimum voltage to injected current ratio (V/I = 0.0005 ohm), minimum apparent resistivity (1 ohm·m), and maximum apparent resistivity (10000 ohm·m). No data were filtered using these criteria, which indicate high field data quality. Mean and standard deviation of error during field operation (normal vs. reversed polarity measurements) were about 0.001 and 0.002 ohm, respectively, whereas mean and standard deviation of contact resistance were 18.13 and 12.63 ohm, respectively.

For the inversion we used two codes, EarthImager 2D (Advanced Geosciences Inc., 2005) and DC2DInvRes (Günther, 2004). In both cases we opted for robust inversion, in which the model fit criterion is the L_1 norm. Regarding the regularization, we chose smooth inversion. While "blocky" inversion might have also been used for the regularization term, we opted for smooth inversion because of parsimony and because we expect water content (and thus electrical conductivity) to increase smoothly towards the water table. In this context, and after some preliminary trials, the λ regularization parameter was fixed at $\lambda = 75$.

The mesh cells were 0.5 m wide (two divisions between electrodes) and 0.28 m high. The depth of investigation, calculated as the median depth of investigation (Edwards, 1977), is 8 m, but resistivity sections were cut at 4 m, since water table remained above this level throughout the study period.

Time-lapse scheme was performed by using the true resistivity model of the previous step as starting model of the subsequent ERT, that is, the inverted resistivity section of ERT T1 was used as starting model for T2 inversion; the resulting model was used as starting model for T3, and so on. Note that, with this scheme, error propagation may have some impact on the following inversions. For the inversion of the first data set with EarthImager 2D, we used the averaged pseudosection as a starting model. The result was used as the starting model of the next data set and so on.

The same was performed for the first data set using DC2DInvRes. However, with this code, we tested an additional "fixed region" constraint for the following data sets, which fixes the resistivity of specified model cells. This feature was applied to ensure that model cells below groundwater table remained unchanged during

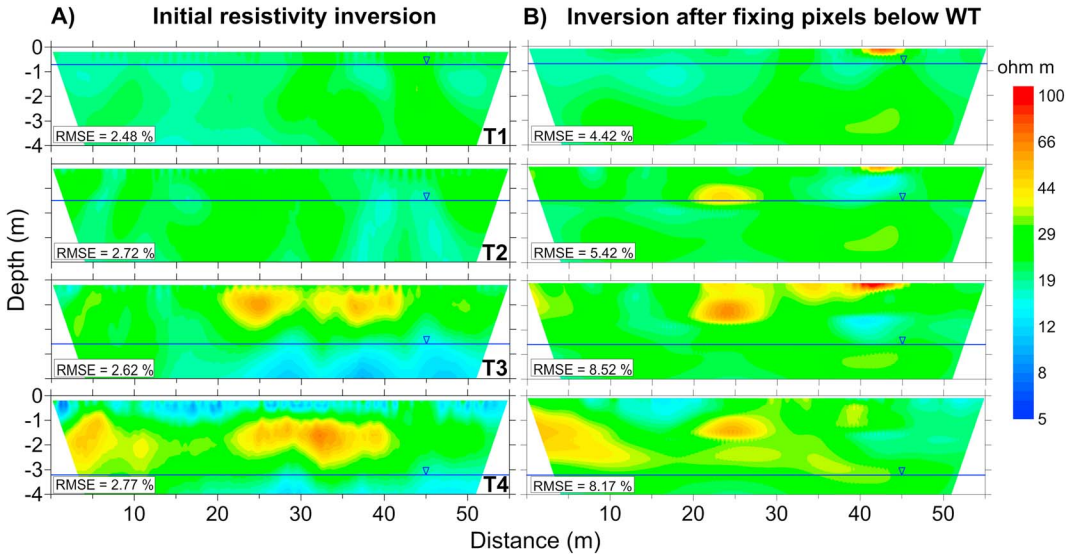

Figure 7. Evolution of soil resistivity observed as water table declined. The position of water table (WT) is also shown. (a) Standard time-lapse resistivity inversion. (b) Inversion after constraining resistivity below the water table to remain fixed to that of the previous tomography.

inversion, that is, we fixed the resistivities at those cells whose middle point falls below the water table to ensure that water content does not change between sequential inversions. Note that errors in the fixed part of the model will cause errors in the inversion since the algorithm tries to compensate for them.

Step 2: Resistivities resulting from inversions were converted to water contents using both Shah and Singh (2005) model and Frohlich and Parke (1989) models (equations (6) and (7)). We fitted our laboratory experiments with these models and obtained the following parameters: (a) c = 2.45, n = 2.14, and ρ_w = 6.06 ohm·m for Shah and Singh's model and (b) n = 1.54, and M = 20.27 (C_s = 0.05 mS/cm) for Frohlich and Parke's one.

Prior to water content calculations, we transformed by interpolation the piece-wise constant resistivity values at each cell (0.5×0.28 m^2) into a smooth field of 0.1×0.1 m^2, by taking the original cell values as point values located in the center of the inversion cells. We followed this approach on the basis that (1) the interpolated resistivities would yield very similar apparent resistivities as the piece-wise constant resulting from inversion, and (2) the resulting resistivity should, in general, be more realistic than the piece-wise constant (water contents and therefore electrical conductivities should increase downwards smoothly).

We compared estimated (ERT) and measured (TDR) water contents to assess the ability of ERT to capture the trends of water content time variability. Since TDR probes are not located exactly over the transect (Figure 5b), we did a statistical comparison. Since TDRs do not cover the whole depth, we restricted the comparison to the TDR interval of measurement (from 30 to 90 cm depth). Thus, for the ERT, we simply multiplied the calculated soil moisture of each cell within this interval times its height (100 mm) to convert soil moisture into water storage (expressed as water column, i.e., in mm). And then, added them up to obtain a unique value of water storage for every x-coordinate in each tomography. We finally extracted statistics (max, min, 1st. quartile, etc.) of water storage for every x-coordinate. We performed these calculations with the two petrophysical laws. The same was done for TDR probes. We multiplied the measured value of water content from each probe by the probe length (150 mm). And again added them up to get a unique value of water storage expressed as water column for the whole interval.

Step 3: We finally estimated Sy by integration of the water content profiles for each x coordinate along the ERT transect using equation (1), as outlined in Figure 1. We performed estimations with both petrophysical laws based on the fixed region constraint resistivities.

4.3. Time-Lapse ERT

Selected resistivity sections are shown in Figure 7. The overall evolution of resistivity is consistent with the water table decline and precipitation during the period shown in Figure 6. Soil resistivity increased in the

upper part of each section as water table declined. Note, however, that a lower resistivity was recorded in the uppermost soil as a consequence of the mid-April 2015 precipitations (Figure 6). These observations confirm the ability of ERT to detect changes in water content.

Two different inversions are included in Figure 7. The standard time-lapse robust inversion was performed first using the code EarthImager 2D (Figure 7a). This yielded an overall reasonable evolution of resistivity. However, a detailed analysis reveals some important inconsistencies. Unexpected changes in soil resistivity can be observed below the water table: a decrease in the interval from 35 through 47 m of T2; some small resistivity increases from 20 to 35 m of T2; a noticeable decrease in resistivity in the 25- to 45-m interval of T3. Since changes in soil water content are not possible below the water table, one might hypothesize about an increase in groundwater salinity, perhaps as a consequence of salts leakage from the upper soil and unsaturated zone. But, unsaturated zone pore water conductivity measurements, extracted by suction cups during the study period (the mean value during this time was 1596 μS/cm with a standard deviation of 439 μS/cm), did not display relevant salinity changes. Instead, we attribute these observed decreases in resistivity to inversion artifacts (i.e., features that result from instability during inversion but do not necessarily reflect real variability). This same effect had also been observed in the synthetic example, even in the noiseless inversion (see second row in Figure 2), which demonstrates that inconsistent resistivities can be obtained during inversion. We suspect that, in this case, these inconsistencies may be a result of regularization.

The fixed region constraint was applied to overcome these artifacts. That is, changes in resistivity were restricted to the zone above the water table while resistivity was constrained to remain unchanged below the water table. To this end we used the code DC2DInvRes. The additional constraints led to larger root-mean-square errors of apparent resistivities (even for the first inversion, which must be attributed to differences in the codes). Yet the option was successful in that many presumed inversion artifacts, obviously those located below the water table, disappeared and a more consistent resistivity distribution was obtained (Figure 4b). However, some possible inversion artifacts persisted. Specifically, the resistivity decrease in the zone extending from 37 to 45 m in ERTs T3 and T4 is inconsistent with the drop in water table. In contrast, resistivity decreases near the surface between 10 and 25 m at ERTs T3 and T4 may be attributed to the precipitations occurred during the last days of the study period.

4.4. Derivation of Volumetric Water Contents From Resistivity Using Petrophysical Relationships

Water content was obtained using both equation (6) (Shah & Singh, 2005) and equation (7) (Frohlich & Parke, 1989) from resistivities calculated with the fixed region constraint. Results are shown in Figure 8 as differences in water content between sequential measurement times only for the case of Shah and Singh's law. Again, overall results are consistent with expected changes in water content during water table decline (Figure 1). With the exception of central zone in T1–T2, the largest change in water content occurs not immediately above the water table, but above the capillary fringe. We do not think that this is an inversion artifact because the fine grained sediments that compound the aquifer and unsaturated zone are expected to develop important capillary rise, which avoid significant changes in water content close to water table. The increase in water content observed in the uppermost soil in the lapse T3–T4 is attributed to the large rainfall event that occurred at the end of the study period (~120 mm a few days before performing ERT T4 survey). The scope of the infiltration front is clearly delimited.

Water content remains unchanged below the water table because resistivity was constrained not to increase at those grid cells. However, some increases in water content were estimated in the area between sequential water tables in the interval from 35 through 47 m at the lapses T1–T2 and T2–T3. Obviously, water content is not expected to increase as the water table drops and therefore, the "natural" explanation is that an inversion artifact is the cause of this "anomalous" zone. In view of the results of the synthetic example, we suspect that this anomaly may also be an inversion artifact.

A small increase in water content was observed in the interval between 10 to 20 m in the lapse T2–T3, just above the water table at T2. Since rainfall in between these surveys was moderate (34 mm 8 days before the survey), one may expect that high evapotranspiration rates at this time of the year should prevent for any increase in soil water content. However, soil heterogeneities, that is, a more retentive zone, may likely be the reason of lesser water losses respect to the surrounding soil. In fact, one should not lose sight of that the increase in water content was 0.02 cm^3/cm^3, which is within the resolution capabilities of the method.

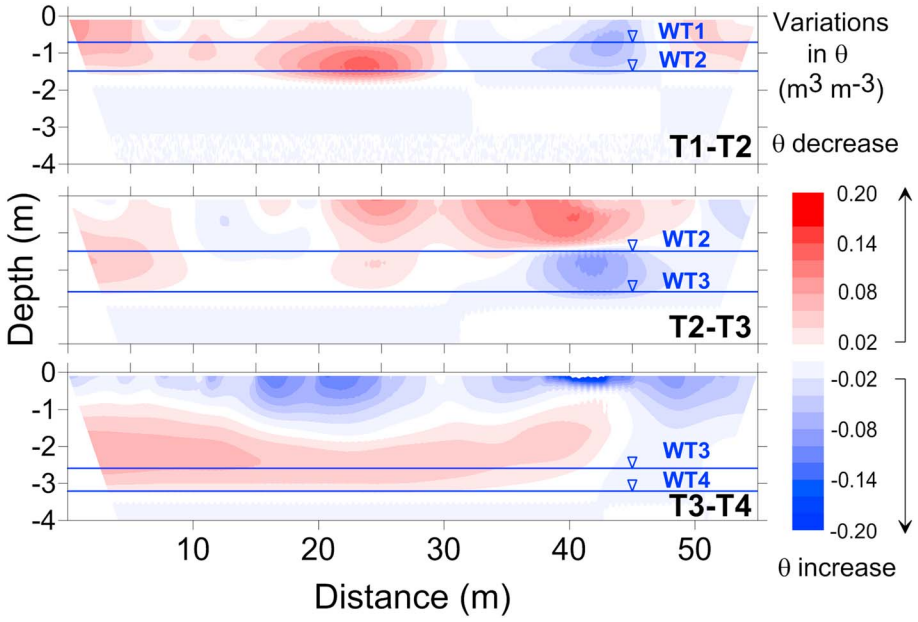

Figure 8. Differences in soil water contents (θ) between successive resistivity sections (T1 to T4) using the inverted resistivity with fixed region constraint. The position of water table (WT) that corresponds to each resistivity measurement is indicated.

Figure 9 displays a comparison between ERT-derived (θ_{ERT}) and TDR-measured (θ_{TDR}) soil water storages between 30 and 90 cm depth, which is the depth range covered by TDR probes. Since these probes were not exactly over the ERT transect (Figure 5b), we compared TDR values to ERT boxplots (of the distributions along *x*). We performed calculation using Shah and Singh (2005, equation 6) and Frohlich and Parke (1989, equation 7) models for inverted resistivities with fixed inversion constraint (DC2DInvRes).

In general terms, evolution trends are consistent with both models. Water contents drop slightly between T1 and T2, more significantly between T2 and T3, and they recover in T4 (recall that T4 was measured shortly after a rainfall event (Figure 6) and that the measurements of Figure 9 are quite shallow). Except for T3 ERT, estimations with Shah and Singh's model are within, or very close to, the interquartile range of ERT. Variability in ERT-derived soil storage was observed to increase as drainage progressed, thus revealing the soil

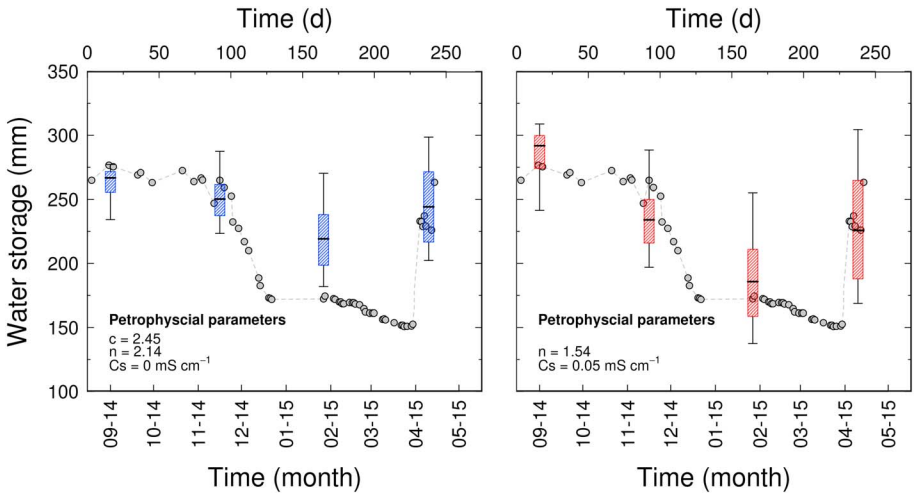

Figure 9. Comparison between time domain reflectometry-measured (points) and electrical resistivity tomography-derived water storage using (left) Shah and Singh (2005) model and (right) Frohlich and Parke (1989) model. Boxplots indicate median, first and third quartile, minimum, and maximum of electrical resistivity tomography water storage along the transect.

heterogeneities. In summer time, however, ERT-derived soil storage overestimated the amount computed with TDR. Since water-resistivity relationship follows an exponential law, a small modification in Shah and Singh's law parameters may provide a better adjustment in this part of high resistivities. On the other hand, Frohlich and Parke's model allowed for greater variations in soil storage with also an increased in dispersivity, that is, a larger interquartile distance. As a consequence, it looks like a better fit was obtained with this law, especially for the summer time, where the median value is very close to TDR estimations. As discussed in section 3.3, the choice of petrophysical law (and also the parameters) is critical for water content and Sy estimation. Still, estimations of water storage by ERT were sensitive enough for both models to reproduce, at least qualitatively (also quantitatively in Frohlich and Parke's model) the TDR changes in water content.

4.5. Estimation of Sy From the Changes in Volumetric Water Content and Groundwater Head

Sy was estimated from the changes in volumetric water content and groundwater head using equation (1). Four $\theta_{ERT}(z)$ profiles, extracted from $x = 25$ m are shown in Figure 10 for different time intervals. $\theta_{ERT}(z)$ derived from fixed region constraint inversion using Shah and Singh's model (equation (6)). The shaded region in Figure 10 indicates the area that was integrated to obtain the Sy value.

All θ_{ERT} profiles show the influence of infiltration and evapotranspiration, which points out that integration should not be performed until the soil surface: the increase in water content due to infiltration will produce an underestimation of Sy, whereas water loses due to evapotranspiration will yield an overestimation of Sy. Therefore, the upper integration limit was set at the depth of ZFP. In the case of Figure 10a, the upper integration limit was the upper water table due to its closeness to soil surface. In the case of Figure 10c, this limit was established at the depth of infiltration front, as defined by ERT (Figure 9). Of course, these assumptions imply uncertainties in the Sy estimation. However, the theoretical displacement of water retention curve due to exclusively water table fall (Figure 1), predicts no significant change in water content in the uppermost part of the curve. Therefore, the use of ZFP as an upper integration limit is a reasonable assumption. In fact, the estimated Sy values for these particular cases were 0.110, 0.047, and 0.108. If the whole T1–T4 interval is adopted, the resulting Sy is 0.09. This latter value involves a larger variation in water table and, therefore, it is representative of a larger profile section.

It is difficult to provide an independent validation of these values because, as discussed in the introduction, there is not fully reliable method to estimate Sy. Still, it is nice that Weinzettel et al. (2005) and Varni et al. (2013) obtained values of 0.07 and 0.09, respectively, for this site, which are consistent with ours. They used variations of the water level fluctuation method, typically adopted to estimate recharge assuming that Sy is known. Therefore, their values must be considered as highly uncertain upper bounds of Sy. Furthermore, their values should also be considered as areal averages over a large area. Therefore, they should not be compared to the point values of Figure 10 but to average values over the whole transect.

The procedure was extended to the full length of the transect to get more representative values and to assess the spatial variability of estimated Sy (Figure 11). Estimations were performed by omitting the values whose differences were lower than zero, due to increases in estimated water content, despite the drop in head. For computations, we used sequential water content sections derived from fixed region constraint inversion using both Shah and Singh's and Frohlich and Parke's models.

As before, the overall results are consistent with previous studies. Note that the application of the method allowed us to estimate both lateral and vertical variations of Sy. Variability is significant, which is consistent with expectations, but is rarely acknowledged. It is hard to qualify the lateral variability. The drop at the right end might well represent the effect of a moisture front localized in that region in response to the rainfall of early May shortly before the T4 campaign, which suggests that it is better to perform the ERT's after a long period without rain. Still, lateral variability of Sy is not surprising in view of the observed textural variations in these sediments. And the increase of Sy with depth is fully consistent with expectations. The deep loessic sediments contain much less clay than the upper edaphic horizons, so that Sy should be expected to increase with depth.

Regarding computations for the whole period, one may expect a more robust estimation since differences in water table are larger and therefore, contrasts in water content tend to be maximum. Values are somewhat in between estimations with T1–T2, and T3–T4, with a mean value of 4.8% for Shah and Singh's law and 10.7% for Frohlich and Parke's one. Besides that, similar trends were observed with a general drop to the right of the

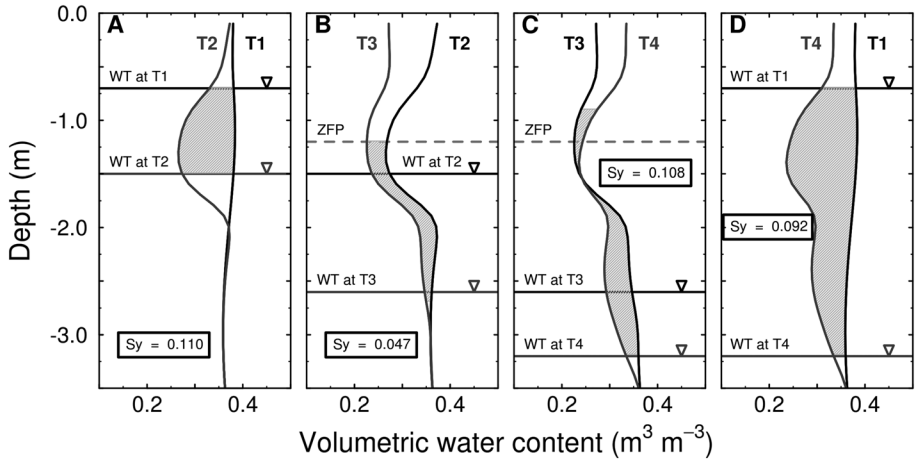

Figure 10. Electrical resistivity tomography-derived soil water content (θ_{ERT}) profiles for (a) times corresponding to T1 and T2, (b) T2 and T3, (c) T3 and T4, and (d) T1 and T4. The shaded region indicates the area that was integrated to obtain specific yield (Sy). The positions of water table (WT) and zero flux plane (ZFP) are indicated.

section. As a consequence of larger soil volume integration to compute Sy, vertical resolution is decreased but representativeness, increased.

It is worth to highlight that, in some cases (intervals T2–T3 and T3–T4), the use of a different petrophysical models does not affect significantly the estimated Sy value. The same was demonstrated with the results of synthetic example (Figure 4), in which we showed that if petrophysical parameters are within the expected values for the site (good calibration) they have a subtle impact on estimated Sy. Still, quite large differences in absolute value (the trends are the same) were observed in the case of T1–T2. The fact that T1 mesh was resized to match T2 mesh may induce some errors in inversion and, therefore, in the resulting Sy value. The estimation for the complete periods (T1–T4) showed similar results. The model of Frohlich and Parke (1989) allows for greater variation in calculated water content (recall Figure 9), which results in larger Sy in all cases, confirming that it is the slope of the petrophysical law what controls the estimated Sy.

5. Discussion

The error analysis showed that accuracy and robustness of the estimation procedure are linked to (1) the integral (along the vertical) nature of the Sy concept and (2) the expected high correlation of moisture content

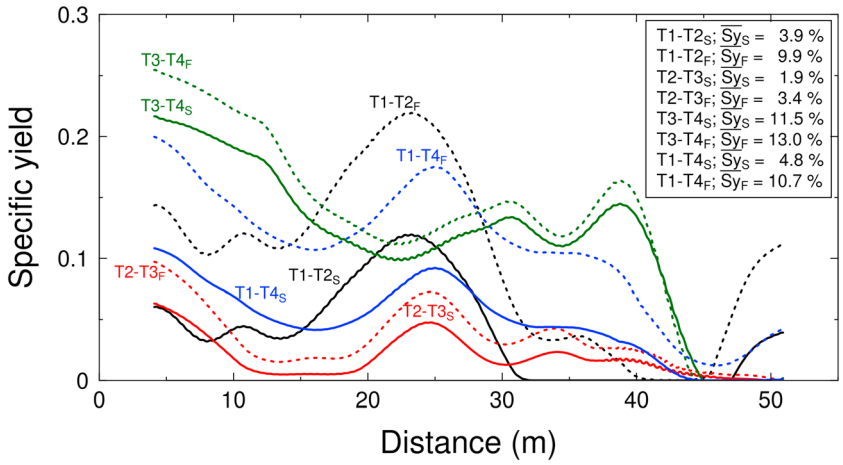

Figure 11. Variation along the transect of specific yield (Sy) calculated from electrical resistivity tomography using Shah and Singh (2005) law (solid lines, subscript "S") or Frohlich and Parke (1989) model (short dashed lines, subscript "F"). Variation in water table depths for periods T1–T2, T2–T3, T3–T4, and T1–T4 were 0.71–1.51, 1.51–2.61, 2.61–3.21, and 0.71–3.21, respectively.

errors (caused by either ERT inversion or petrophysical parameters) at sequential surveys, which tend to cancel during the computation of Sy.

These findings were confirmed by the synthetic example, which demonstrated more clearly than the error analysis that the method is very robust with respect to inversion errors. On the one hand, high-frequency inversion errors tend to cancel during integration (of moisture) along vertical profiles. Still, low frequency errors translated into spatial fluctuations of estimated Sy when inversion errors were high (i.e., when a large noise was added to V/I measurements). Furthermore, inversion errors of sequential surveys are highly correlated and tend to cancel during calculation of Sy. This is true for systematic errors that use to be the most important source of noise during inversion but remains so even when a moderate purely random component is added to every measurement. This implies that is important to ensure that electrodes are located at identical positions between sequential surveys (i.e., by maintaining a fixed electrode network during the set of surveys).

Petrophysical parameters may have a significant impact on the final Sy value. The key issue here is whether the overall slope of the petrophysical law (bulk conductivity versus saturation) is correct. A wrong slope implies that for a given change in resistive during sequential campaigns, the computed change in water content will be wrong. This indicates that calibration of the petrophysical law on site samples is essential for success and that calibration efforts should concentrate on the expected variation of water content. This type of error affects the overall Sy value, but variability patterns were very well identified even when the petrophysical law was poor.

Applicability of the method was tested at a field site, where four ERT surveys were carried out along a transect while water table declined from 0.71 to 3.21 m below surface. The proposed method yielded the overall value of Sy and its lateral and vertical variability. It is hard to validate these results because no reliable method is available for the estimation of Sy, but our results are consistent with all available information. The overall average Sy values were comparable to those derived by variants of the water level fluctuation method. The computed lateral variability should be considered reasonable, as it was similar for sequential estimations and it is consistent with the patterns of textural variability at the site. The computed vertical variability of Sy should also be considered reasonable. Local sediments tend to be less retentive at depth, which agrees with the increased values of Sy.

Despite this promising outlook, it is clear that difficulties still remain regarding both the Sy definition itself, and the application of the method we are proposing. For one thing, a poor choice of petrophysical law may lead to biased estimation of average Sy. Yet, even in those cases, the spatial variability patterns are generally well captured.

While the method appears effective, there is plenty of room for improvement. Standard time-lapse inversion yielded some spurious resistivities, which were also observed even in the noiseless inversion of the synthetic example. Spurious artifacts include the decreasing resistivities below the water table. These artifacts could be overcome by applying the fixed region constraint, which led to a significant overall improvement. But some fluctuations still remained in the zone between 35 and 47 from *x*-coordinate origin. In view of the results of synthetic example, these fluctuations could be attributed to preferential flow path, but they may also be spurious. In fact, a problem with the fixed region constraint is that errors in the resistivities of the first image will be translated to sequential inversions and, moreover, that errors in the fixed part of the model will cause errors in the inversion as the algorithm tries to compensate for them. Therefore, much can be gained by improving the inversion method. For example, it may be worth to consider the joint inversion of all images while imposing that resistivities below the water table are the same in all of them. Also, we did not analyze the impact of salinity and temperature variability on the estimation of Sy. However, the error analysis suggests that it may be relevant when either of them change along time (e.g., temperature) or space (both may change with depth; see Jayawickreme et al., 2010). While we had no indications of significant variability at our site, efforts at characterizing their variability will also improve results.

Another avenue of improvement would be the use of joint inversion of different types of signals in a unique estimation process (Zhdanov et al., 2012). This approach has been used with a certain degree of success to integrate different geophysical methods: DC resistivity and magnetotelluric (Vozoff & Jupp, 1975), gravity and magnetics (Shamsipour et al., 2012), gravity-gradient and borehole gravity (Meixia et al., 2015), and seismic and electromagnetic imaging (Hoversten et al., 2003). Joint inversion of GPR and ERT data sound

especially promising for our problem (Doetsch et al., 2010). Also relevant would be to couple ERT inversion to unsaturated flow modeling for a long time interval or during a pumping test, which should alleviate problems with the petrophysical law (and help in the estimation of a field scale law!). Variations of coupled inversion of geophysical and hydrological data have proven useful (Fowler & Moysey, 2011; Kowalsky et al., 2005; Rucker, 2011), although algorithmic improvements are required to make it practical (Linde et al., 2006). Joint inversion of, for instance, response to a long pumping test would guarantee internal consistence with volumetric water data and facilitate overcoming the bias caused by erroneous petrophysical law parameters.

6. Conclusions

We have proposed a method to derive Sy and its space and time variability from time-lapse ERT surveys during periods of significant head drop or rise. We have analyzed the validity and robustness of the method through error analysis, a synthetic simulation and a real case application. The key points resulting from these analyses are that

1. The method is accurate and robust with respect to inversion errors because Sy estimation integrates the inversion results, so that high-frequency inversion errors tend to cancel. Moreover, Sy is obtained by subtraction of sequential inversions, so that systematic errors also tend to cancel.
2. Petrophysical parameters may affect the final Sy value. Efforts should focus in calibration especially in the range between saturation and field capacity, where petrophysical law errors translate directly onto errors in Sy estimation.
3. The Sy variability patterns were well reproduced in our synthetic example, even in the presence of errors in the petrophysical law, which tend to affect more the overall Sy value than its variability.
4. By treating the unsaturated zone as whole, the proposed method may be used to overcome some of the conceptual difficulties of Sy (closeness to the surface, delayed yield, spatial variability).

In summary, the proposed approach provides a picture of how, how much, and where water is being released from the soil, which is the ultimate goal of the Sy concept to begin with. Still, inversion improvements, possibly coupled to other geophysical techniques and/or unsaturated zone flow simulation, are required to reduce uncertainty. What is clear is that Sy is a spatially and temporally variable parameter, whose estimation is very difficult. We believe that the results presented here demonstrate that ERT represents a possible avenue to obtain reliable Sy estimates, to account for such variability and to facilitate addressing the conceptual difficulties associated to the Sy concept.

Acknowledgments
The manuscript has improved significantly during the review process as a result of comments from Lee Slater, Remke L. Van Dam, Larry Bentley, Dale Rucker, and Niels Claes. Funding for this research was provided by the Agencia Nacional de Promoción Científica y Tecnológica, Argentina (Projects PID 0075/2011 and Project PICT 1805/2014) and Consejo Hídrico Federal (COHIFE, Project PID 0075/2011). The second author wants to acknowledge funding from the Spanish CICYT projects MEDISTRAES (grant agreements CGL2013-48869 and CGL2016-77122). The data sets used in this work are available as supporting information.

References

Advanced Geosciences Inc. (2005). EarthImager 2D, resistivity and IP inversion software, version 2.2.8. Instruction manual. Advanced Geosciences, Austin, TX. 139 p.

Archie, G. E. (1942). The electrical resistivity log as an aid in determining some reservoir characteristics. *Transactions of the American Institute of Mining and Metallurgical Engineers*, *146*, 54–62.

Boulton, N. S. (1963). Analysis of data from non-equilibrium pumping tests allowing for delayed yield from storage. *Proceedings of the Institution of Civil Engineers*, *26*, 469–482.

Carrera, J., & Neuman, S. P. (1986). Estimation of aquifer parameters under transient and steady state condition: 1. Maximum likelihood method incorporating prior information. *Water Resources Research*, *22*(2), 199–210. https://doi.org/10.1029/WR022i002p00199

Carsel, R. F., & Parrish, R. S. (1988). Developing joint probability distributions of soil water retention characteristics. *Water Resources Research*, *24*(5), 755–769. https://doi.org/10.1029/WR024i005p00755

Childs, E. C. (1960). The nonsteady state of the water table in drained land. *Journal of Geophysical Research*, *65*(2), 780–782. https://doi.org/10.1029/JZ065i002p00780

Claerbout, J. F., & Muir, F. (1973). Robust modeling with erratic data. *Geophysics*, *38*(5), 826–844. https://doi.org/10.1190/1.1440378

Damiata, B. N., & Lee, T. C. (2006). Simulated gravitational response to hydraulic testing of unconfined aquifers. *Journal of Hydrology*, *318*(1-4), 348–359. https://doi.org/10.1016/j.jhydrol.2005.06.024

deGroot-Hedlin, C., & Constable, S. (1990). Occam's inversion to generate smooth, two-dimensional models from magnetotelluric data. *Geophysics*, *55*(12), 1613–1624. https://doi.org/10.1190/1.1442813

Dietrich, S., Weinzettel, P., & Varni, M. (2014). Infiltration and drainage analysis in a heterogeneous soil by electrical resistivity tomography. *Soil Science Society of America Journal*, *78*(4), 1153–1167. https://doi.org/10.2136/sssaj2014.02.0062

Doetsch, J., Linde, N., & Binley, A. (2010). Structural joint inversion of time-lapse crosshole ERT and GPR traveltime data. *Geophysical Research Letters*, *37*, L24404. https://doi.org/10.1029/2010GL045482

dos Santos, A. G. Jr. & Youngs, E. G. (1969). A study of the specific yield in land-drainage situations. *Journal of Hydrology*, *8*: 59–81, 1. https://doi.org/10.1016/0022-1694(69)90031-6

Duke, H. R. (1972). Capillary properties of soils—Influence upon specific yield. *Transactions of the American Society of Agricultural Engineers*, *15*(4), 0688–0691. https://doi.org/10.13031/2013.37986

Edwards, L. S. (1977). A modified pseudosection for resistivity and IP. *Geophysics*, *42*(5), 1020–1036. https://doi.org/10.1190/1.1440762

El-Diasty, M. (2016). Groundwater storage change detection using micro-gravimetric technology. *Journal of Geophysics and Engineering*, *13*, 259–272. https://doi.org/10.1088/1742-2132/13/3/259

Ellis, R. G., & Oldenburg, D. W. (1994). Applied geophysical inversion. *Geophysical Journal International*, *116*(1), 5–11. https://doi.org/10.1111/j.1365-246X.1994.tb02122.x

Farquharson, C. G., & Oldenburg, D. W. (1998). Non-linear inversion using general measures of data misfit and model structure. *Geophysical Journal International*, *134*(1), 213–227. https://doi.org/10.1046/j.1365-246x.1998.00555.x

Fowler, D. E., & Moysey, S. M. J. (2011). Estimation of aquifer transport parameters from resistivity monitoring data within a coupled inversion framework. *Journal of Hydrology*, *409*(1-2), 545–554. https://doi.org/10.1016/j.jhydrol.2011.08.063

Friedman, S. P. (2005). Soil properties influencing apparent electrical conductivity: A review. *Computers and Electronics in Agriculture*, *46*(1-3), 45–70. https://doi.org/10.1016/j.compag.2004.11.001

Frohlich, R. K., & Kelly, W. E. (1988). Estimates of specific yield with the geoelectric resistivity method in glacial aquifers. *Journal of Hydrology*, *97*(1–2), 33–44. https://doi.org/10.1016/0022-1694(88)90064-9

Frohlich, R. K., & Parke, C. D. (1989). The electrical resistivity of the vadose zone—Field survey. *Ground Water*, *27*(4), 524–530. https://doi.org/10.1111/j.1745-6584.1989.tb01973.x

Gehman, C. L., Harry, D. L., Sanford, W. E., Stednick, J. D., & Beckman, N. A. (2009). Estimating specific yield and storage change in an unconfined aquifer using temporal gravity surveys. *Water Resources Research*, *45*, W00D21. https://doi.org/10.1029/2007WR006096

Gillham, R. W. (1984). The capillary fringe and its effect on water-table response. *Journal of Hydrology*, *67*(1-4), 307–324. https://doi.org/10.1016/0022-1694(84)90248-8

Glover, P. W. J. (2015). Geophysical properties of the near surface earth: Electrical properties. In *Treatise geophys* (2nd. ed., Vol. 189, pp. 89–137). Leeds, UK: University of Leeds.

Günther, T. (2004). Inversion methods and resolution analysis for the 2D/3D reconstruction of resistivity structures from DC measurements, PhD theses. University of Mining and Technology, Freiberg, Germany.

Hayley, K., Pidlisecky, A., & Bentley, L. R. (2011). Simultaneous time-lapse electrical resistivity inversion. *Journal of Applied Geophysics*, *75*(2), 401–411. https://doi.org/10.1016/j.jappgeo.2011.06.035

Healy, R. W., & Cook, P. G. (2002). Using groundwater levels to estimate recharge. *Hydrogeology Journal*, *10*(1), 91–109. https://doi.org/10.1007/s10040-001-0178-0

Hillel, D. (1998). *Environmental soil physics*. San Diego, CA: Academic Press.

Hoversten, G. M., Gritto, R., Washbourne, J., & Daley, T. (2003). Pressure and fluid saturation prediction in a multicomponent reservoir using combined seismic and electromagnetic imaging. *Geophysics*, *68*(5), 1580–1591. https://doi.org/10.1190/1.1620632

Jayawickreme, D. H., Van Dam, R. L., & Hyndman, D. W. (2010). Hydrological consequences of land-cover change: Quantifying the influence of plants on soil moisture with time-lapse electrical resistivity. *Geophysics*, *75*(4), WA43–WA50. https://doi.org/10.1190/1.3464760

Kowalsky, M. B., Finsterle, S., Peterson, J., Hubbard, S., Rubin, Y., Majer, E., et al. (2005). Estimation of field-scale soil hydraulic and dielectric parameters through joint inversion of GPR and hydrological data. *Water Resources Research*, *41*, W11425. https://doi.org/10.1029/2005WR004237

Legchenko, A., & Valla, P. (2002). A review of the basic principles for proton magnetic resonance sounding measurements. *Journal of Applied Geophysics*, *50*(1-2), 3–19. https://doi.org/10.1016/S0926-9851(02)00127-1

Linde, N., Binley, A., Tryggvason, A., Pedersen, L. B., & Revil, A. (2006). Improved hydrogeophysical characterization using joint inversion of cross-hole electrical resistance and ground-penetrating radar traveltime data. *Water Resources Research*, *42*, W12404. https://doi.org/10.1029/2006WR005131

Loetz, O. J., & Leake, S. A. (1983). A method for estimating groundwater return flow to the lower Colorado River in the Yuma area, Arizona and California—Executive Summary. U.S. Geol. Surv., Water Resour. Invest. Report, 83–4221, 86 pp., Tucson, Arizona.

Loke, M. H., Acworth, I., & Dahlin, T. (2003). A comparison of smooth and blocky inversion methods in 2D electrical imaging surveys. *Exploration Geophysics*, *34*(3), 182–187. https://doi.org/10.1071/EG03182

Loke, M. H., Dahlin, T., & Rucker, D. F. (2014). Smoothness-constrained time-lapse inversion of data from 3-D resistivity surveys. *Near Surface Geophysics*, *12*(1), 5–24.

Mathias, S. A., & Butler, A. P. (2006). Linearized Richards' equation approach to pumping test analysis in compressible aquifers. *Water Resources Research*, *42*, W06408. https://doi.org/10.1029/2005WR004680

Meier, P. M., Carrera, J., & Sanchez-Vila, X. (1998). An evaluation of Jacob's method for the interpretation of pumping tests in heterogeneous formation. *Water Resources Research*, *34*(5), 1011–1025. https://doi.org/10.1029/98WR00008

Meinzer, O. (1923). Outline of ground-water hydrology with definitions. In *U.S. Geol. Survey Water Supply·Paper, 494* (71 pp.). Washington, DC: US Government Printing Office.

Meinzer, O. (1932). Outline of methods for estimating ground-water supplies. *U.S. Geological Survey Water Supply Paper, 638-C* (144 pp.). Washington, DC: US Government Printing Office.

Meixia, G., Qingjie, Y., & Danian, H. (2015). 3D joint inversion of gravity-gradient and borehole gravity data. *Exploration Geophysics*. https://doi.org/10.1071/EG15023

Meyer, W. R. (1962). Use of a neutron moisture probe to determine the storage coefficient of an unconfined aquifer: *U.S. Geol. Surv. Prof. Paper*, 450-E: 174–176.

Miller, C. R., Routh, P. S., Brosten, T. R., & McNamara, J. P. (2008). Application of time-lapse ERT imaging to watershed characterization. *Geophysics*, *73*, 7–17.

Moench, A. F. (1994). Specific yield as determined by type curve analysis of aquifer test data. *Ground Water*, *32*(6), 949–957.

Moench, A. F. (2008). Analytical and numerical analyses of an unconfined aquifer test considering unsaturated zone characteristics. *Water Resources Research*, *44*, W06409. https://doi.org/10.1029/2006WR005736

Neuman, S. P. (1975). Analysis of pumping test data from anisotropic unconfined aquifers considering delayed gravity response. *Water Resources Research*, *11*(2), 329–342. https://doi.org/10.1029/WR011i002p00329

Neuman, S. P. (1979). Perspective on 'delayed yield'. *Water Resources Research*, *15*(4), 899–908. https://doi.org/10.1029/WR015i004p00899

Neuman, S. P. (1987). On methods of determining specific yield. *Ground Water*, *25*(6), 679–684.

Niwas, S., Tezkan, B., & Israil, M. (2011). Aquifer hydraulic conductivity estimation from surface geoelectrical measurements for Krauthausen test site, Germany. *Hydrogeology Journal*, *19*(2), 307–315.

Nwankwor, G. I., Cherry, J. A., & Gillham, R. W. (1984). A comparative study of specific yield determinations for shallow sand aquifer. *Ground Water*, *22*(6), 764–772.

Oberdörster, C., Vanderborght, J., Kemna, A., & Vereecken, H. (2010). Investigating preferential flow processes in a forest soil using time domain reflectometry and electrical resisti vity tomography. *Vadose Zone Journal*, *9*, 350–361.
Oldenborger, G. A., Knoll, M. E., Routh, P. S., & LaBrecque, D. J. (2007). Time-lapse ERT monitoring of an injection/withdrawal experiment in a shallow unconfined aquifer. *Geophysics*, *72*(4), F177–F187.
Oldenborger, G. A., Routh, P. S., & Knoll, M. D. (2005). Sensitivity of electrical resistivity tomography data to electrode position errors. *Geophysical Journal International*, *163*, 1–9.
Plata, J., & Rubio, F. (2011). The potential of the qualitative interpretation of MRS data: hydrogeophysical study of the Lagoons of Estaña (Spain). *Geophysics*, *9*(2), 225–240.
Remson, I., & Lang, S. M. (1955). A pumping-test method for the determination of specific yield. *Transactions - American Geophysical Union*, *36*(2), 321–325.
Revil, A., & Cathles, L. M. III (1999). Permeability of shaly sand. *Water Resources Research*, *35*(3), 651–662.
Rinaldi, V. A., & Cuestas, G. A. (2002). Ohmic conductivity of a compacted silty clay. *Journal of Geotechnical and Geoenviromental Engineering*, *128*, 824–835.
Rucker, D. F. (2009). A coupled electrical resistivity-infiltration model for wetting front evaluation. *Vadose Zone Journal*, *8*(2), 383–388.
Rucker, D. F. (2011). Inverse upscaling of hydraulic parameters during constant flux infiltration using borehole radar. *Advances in Water Resources*, *34*(2), 215–226.
Samouëlian, A., Cousin, I., Tabbagh, A., Bruand, A., & Richard, G. (2005). Electrical resistivity survey in soil science: A review. *Soil and Tillage Research*, *83*, 173–193.
Sanchez-Vila, X., Meier, P. M., & Carrera, J. (1999). Pumping tests in heterogeneous aquifers: An analytical study of what can be obtained from their interpretation using Jacob's method. *Water Resources Research*, *35*(4), 943–952. https://doi.org/10.1029/1999WR900007
Shah, P. H., & Singh, D. N. (2005). Generalized Archie's law for estimation of soil electrical conductivity. *Journal of ASTM International*, *2*(5), 1–20.
Shamsipour, P., Marcotte, D., & Chouteau, M. (2012). 3D stochastic joint inversion of gravity and magnetic data. *Journal of Applied Geophysics*, *79*, 27–37.
Silberstein, R. P., Dawes, W. R., Bastow, T. P., Byrne, J., & Smart, N. F. (2013). Evaluation of changes in post-fire recharge under native woodland using hydrological measurements, modelling and remote sensing. *Journal of Hydrology*, *489*, 1–15.
Singha, K., & Gorelick, S. M. (2005). Saline tracer visualized with three-dimensional electrical resistivity tomography: Field-scale spatial moment analysis. *Water Resources Research*, *41*, W05023. https://doi.org/10.1029/2004WR003460
Slater, L., Binley, A. M., Daily, W., & Johnson, R. (2000). Cross-hole electrical imaging of a controlled saline tracer injection. *Journal of Applied Geophysics*, *44*(2–3), 85–102.
Soil Survey Staff (1999). *Soil taxonomy. A basic system of soil classification for making and interpreting soil surveys*, *Agric. Handbook No. 436*, (2nd ed., p. 869). Washington, DC: NRCS-USDA. U.S. Gov. Print. Office.
Tartakovsky, G. D., & Neuman, S. P. (2007). Three-dimensional saturated-unsaturated flow with axial symmetry to a partially penetrating well in a compressible unconfined aquifer. *Water Resources Research*, *43*, W01410. https://doi.org/10.1029/2006WR005153
Tizro, A. T., Voudouris, K., & Basami, Y. (2012). Estimation of porosity and specific yield by application of Geoelectrical method—A case study in western Iran. *Journal of Hydrology*, *454–455*, 160–172.
Tripp, A. C., Hohmannt, G. W., & Swift, C. M. Jr. (1984). Two-dimensional resistivity inversion. *Geophysics*, *49*(10), 1708–1717.
Usunoff, E., Varni, M., Weinzettel, P., & Rivas, R. (1999). Hidrogeología de grandes llanuras: La pampa húmeda Argentina (In Spanish, with English abstract). *Boletín del Instituto geológico y minero de España*, *110*, 391–406.
van Gaalen, J. F., Kruse, S., Lafrenz, W. B., & Burroughs, S. M. (2013). Predicting water table response to rainfall events, central Florida. *Ground Water*, *51*(3), 350–362.
van Genuchten, M. T. (1980). A closed-form equation for predicting the hydraulic conductivity of unsaturated soils. *Soil Science Society of America Journal*, *44*, 892–898.
Varni, M., Comas, R., Weinzettel, P., & Dietrich, S. (2013). Application of water table fluctuation method to characterize the groundwater recharge in the Pampa plain, Argentina. *Hydrological Sciences Journal*, *58*(7), 1445–1455.
Varni, M. R., & Usunoff, E. J. (1999). Simulation of regional-scale groundwater flow in the Azul River basin, Buenos Aires Province, Argentina. *Hydrogeology Journal*, *7*, 180–187.
Vouillamoz, J. M., Chatenoux, B., Mathieu, F., Baltassat, J. M., & Legchenko, A. (2007). Efficiency of joint use of MRS and VES to characterize coastal Aquifer in Myanmar. *Journal of Applied Geophysics*, *6*, 142–154.
Vouillamoz, J. M., Lawson, F. M. A., Yalo, N., & Descloitres, M. (2014). The use of magnetic resonance sounding for quantifying specific yield and transmissivity in hard rock aquifers: The example of Benin. *Journal of Applied Geophysics*, *107*, 16–24.
Vozoff, K., & Jupp, D. L. B. (1975). Joint inversion of geophysical data. *Geophysical Journal of the Royal Astronomical Society*, *42*, 977–991.
Wehrer, M., & Slater, L. D. (2015). Characterization of water content dynamics and tracer breakthrough by 3-D electrical resistivity tomography (ERT) under transient unsaturated conditions. *Water Resources Research*, *51*, 97–124. https://doi.org/10.1002/2014WR016131
Weinzettel, P., Usunoff, E., & Vives, L. (2005). Groundwater recharge estimations from studies of the unsaturated zone. In E. Bocanegra, M. Hernandez, & E. Usunoff (Eds.), *Groundwater and human development* (262 pp.). Leiden: Balkema.
Weinzettel, P., Varni, M., & Dietrich, S. (2009). Evaluación de tres dispositivos de tomografía eléctrica para la identificación de horizontes petrocálcicos en el suelo (In Spanish, with English abstract). *Ciencia del Suelo*, *27*, 135–146.
Wilkinson, P. B., Chambers, J. E., Lelliott, M., Wealthall, G. P., & Ogilvy, R. D. (2008). Extreme sensitivity of crosshole electrical resistivity tomography measurements to geometric errors. *Geophysical Journal International*, *173*(1), 49–62.
Willmann, M., Carrera, J., & Sánchez-Vila, X. (2008). Transport upscaling in heterogeneous aquifers: What physical parameters control memory functions? *Water Resources Research*, *44*, W12437. https://doi.org/10.1029/2007WR006531
Winsauer, W. O., Shearin, H. M. Jr., Masson, P. H., & Williams, M. (1952). Resistivity of brine-saturated sands in relation to pore geometry. *AAPG Bulletin*, *36*(2), 253–277.
Zárate, M. A. (2003). Loess of southern South America. *Quaternary Science Reviews*, *22*, 1987–2006.
Zhdanov, M. S., Gribenko, A. V., Wilson, G. A., & Funk, C. (2012). 3D joint inversion of geophysical data with Gramian constraints: A case study from the Carrapateena IOCG deposit, South Australia. *The Leading Edge*, *31*(11), 1382–1388.
Zhou, B., & Dahlin, T. (2003). Properties and effects of measurement errors on 2D resistivity imaging surveying. *Near Surface Geophysics*, *1*(3), 105–117.